PHOTONICS Research

Observation of transition between multimode Q-switching and spatiotemporal mode locking

Kewei Liu,[1] Xiaosheng Xiao,[2,3] and Changxi Yang[1,4]

[1]State Key Laboratory of Precision Measurement Technology and Instruments, Department of Precision Instruments, Tsinghua University, Beijing 100084, China
[2]State Key Laboratory of Information Photonics and Optical Communications, School of Electronic Engineering, Beijing University of Posts and Telecommunications, Beijing 100876, China
[3]e-mail: xsxiao@bupt.edu.cn
[4]e-mail: cxyang@tsinghua.edu.cn

Received 6 December 2020; revised 2 February 2021; accepted 2 February 2021; posted 2 February 2021 (Doc. ID 416523); published 24 March 2021

We report experimental observation of multimode *Q*-switching and spatiotemporal mode locking in a multimode fiber laser. A typical steady *Q*-switching state is achieved with a 1.88 μs pulse duration, a 70.14 kHz repetition rate, and a 215.8 mW output power, corresponding to the single pulse energy of 3.08 μJ. We find weak spatial filtering is essential to obtain stable *Q*-switched pulses, in contrast to the relatively stronger spatial filtering for spatiotemporal mode locking. Furthermore, a reversible transition process, as well as a critical bistable state, between multimode *Q*-switching and spatiotemporal mode locking, is achieved with specific spatial coupling and waveplates sets. We believe the results will not only contribute to understanding the complicated nonlinear dynamics in multimode, fiber-based platforms, but also benefit the development of promising high-pulse energy lasers.

https://doi.org/10.1364/PRJ.416523

1. INTRODUCTION

Q-switching (QS) and mode-locking (ML) are two fundamental operating regimes in pulsed lasers [1]. ML originates from the fixed phase relation (synchronization) of multiple longitudinal oscillating modes [2] while QS is a consequence of the modulation of the cavity *Q*-factor by reiteratively emptying and replenishing the stored cavity energy [3]. Tremendous effort has been made during the years to develop efficient saturable absorbers (SAs) to achieve QS [4–6] or ML [3,7–9] in lasers with high performance. Early theoretical analysis modeled the two regimes (i.e., QS and ML) in laser cavities through nonlinear polarization rotation (NPR) [10]. It is noteworthy that recent research that provides links between QS and ML experimentally investigated a novel buildup process of ML via QS by real-time characterization in a fiber laser, throwing light on some dynamics within the QS–ML transition [11]. All these investigations are based on single transverse-mode platforms.

In fact, there have been several investigations dealing with multimode issues, but mostly in the context of QS in solid lasers [12,13] and lately in a few-mode fiber cavity [14]. In addition, multimode fibers (MMFs) have been lately proven to be qualified SAs based on nonlinear multimode interference, facilitating QS [15] and ML [16–18] in fiber lasers. These lasers are essentially operated with a single transverse mode. As for multimode ML, however, a number of transverse modes along with the longitudinal modes nonlinearly interact in a more involved manner, wherein the spatial dimension becomes a crucial factor. Because of the inherent high-dimensional properties of multimode lasers, they provide ideal platforms to look into the complex nonlinear science and connect the nonlinear dynamics to various real-world physical phenomena. Remarkably, the recent successful demonstration of spatiotemporal ML (STML) in multimode fiber lasers [19] has opened up a new frontier of mode-locking and high-dimensional nonlinear dynamics. Then, a series of works related to STML were reported, including work on soliton molecules [20], self-similaritons [21], multiple pulses [22], wavelength-switchable pulses and hysteresis [23], dispersion-managed solitons [24], and vortices [25]. STML has also been realized in an all-fiber cavity using a multimode-fiber-based spectral filter [26] and achieved in cavities composed of MMF with a large modal dispersion [27]. In addition, near single-mode outputs were achieved by optimizing the spatiotemporal evolution in multimode lasers [27,28]. Despite current challenges to fully understand STML, a heuristic theoretical model has been put forward that is adaptive to more general cases, giving much insight into the mechanisms behind STML [29]. The boundaries of multimode fiber lasers are constantly being broadened over the years, showing abundant curiosities and promising perspectives.

Nevertheless, there are few investigations on multimode QS in full-multimode fiber lasers, especially concerning the relation between multimode QS and STML.

In this paper, we report the experimental observation of steady multimode QS states and STML in a multimode fiber laser. Stable multimode QS operation is realized, with a typical result of a 1.88 μs pulse duration and a 70.14 kHz repetition rate. The output power is 215.8 mW, corresponding to the single pulse energy of 3.08 μJ. We find weak spatial filtering (or large spatial filter size) facilitates the formation of multimode QS, compared to the stronger spatial filtering strength to maintain STML in the same cavity. With an appropriate setup of spatial filtering and the SA (i.e., the NPR states), a reversible multimode QS–ML transition is achieved. The transition process can be tuned merely by changing the pump power, given fixed cavity settings. Furthermore, by carefully adjusting the waveplates and pump power, we realize a bistable state between multimode QS and STML. The spatial, spectral, and temporal properties of the output change as the laser operating regime switches in the QS–ML bistable state, without analogues in conventional single transverse-mode lasers. It is the first time, to the best of our knowledge, that the realization of the transition between multimode QS and STML as well as the QS–ML bistable state is reported.

2. EXPERIMENTAL SETUP

The schematic of the experimental setup is shown in Fig. 1, which is similar to our previous layout for an STML demonstration [27]. A 980 nm diode laser is used as the pump source, combining with the signal light by a short-pass dichroic mirror (SPDM). The 0.55 m long multimode step-index gain fiber has a core diameter of 20 μm (LMA-YDF-20/125-9M, NA = 0.08, Nufern, East Granby, CT, USA), supporting up to six transverse modes. A segment of 5.35 m passive graded-index multimode fiber (OM4, with core/cladding diameter of 50/125 μm and supporting ~100 modes, YOFC, Wuhan, China) is spliced to the gain fiber with high refractive index resin glue applied to the joint of the two fiber segments to leak the superfluous pump light. The laser loop is completed with one mirror (M) to couple signal light back to the gain fiber. Note that this coupling serves as a spatial filter since only part of the returning light can couple back into the gain fiber due to its small diameter. A spectral filter is also introduced into the cavity facilitating ML in the normal dispersive waveband. The artificial SA is based on NPR with one half-wave plate and two quarter-wave plates, as illustrated in the schematic. The laser cavity is fully multimode, especially with multiple transverse modes excited in the gain fiber, which has been already demonstrated in our previous work concerning STML [27]. The temporal, spectral, and radio frequency (RF) data of the laser output are acquired by a photodetector with a 5 GHz bandwidth, an oscilloscope (Infiniium DSO80204B, 8G bandwidth, up to 40 GHz sampling rate, Agilent Technologies, Santa Clara, CA, USA; Agilent is now Keysight Technologies, Inc., Santa Rosa, CA, USA), an optical spectrum analyzer [86142B, 0.06 nm spectral resolution, Agilent (now Keysight Technologies)], and an RF signal analyzer [N9020A, Agilent (now Keysight Technologies)], respectively. In addition, beam profiles are captured by an infrared beam analyzer (CinCam CMOS-1201-IR, Cinogy Technologies GmbH, Duderstadt, Germany).

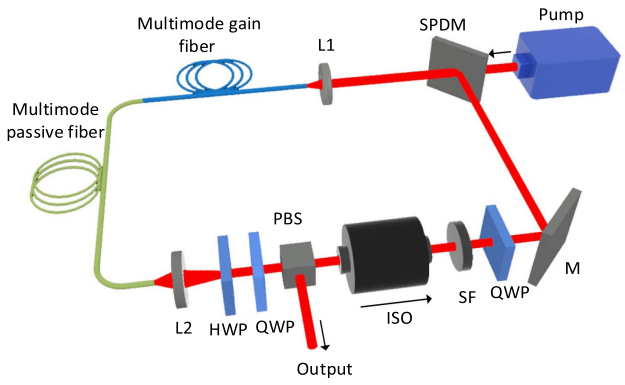

Fig. 1. Schematic of the multimode fiber cavity setup. SPDM, short-pass dichroic mirror; L1 and L2, collimating lens; M, reflective mirror; HWP, half-wave plate; QWP, quarter-wave plate; PBS, polarized beam splitter; ISO, isolator; and SF, spectral filter.

3. RESULTS

A. Multimode QS

To initiate the QS state, the cavity output first needs to achieve a relatively higher power level by adjusting both the rotation angles of the three waveplates and the effective spatial filter size. In other words, the QS state is dependent on both the NPR effect and the spatial filtering strength. Note that the collimating lens 2 (L2) is fixed to two three-axis movable stages, facilitating the control of spatial filtering effect by moving the stage (i.e., equivalent control of the spatial filter size). After the output power reaches its maximum, we slightly rotate the waveplates, and then stable QS pulses are easy to generate. According to our experiment, the influence of the spatial filter size is significant in achieving stable QS states, since the laser can hardly support a QS regime with a smaller spatial filter size configuration. We speculate that a weak spatial filtering effect allows more transverse modes, especially high-order modes, to propagate in the cavity; thus, these transverse modes are able to occupy a larger area of the gain medium, facilitating the higher energy accumulation responsible for QS operation. In contrast, STML usually requires sufficient spatial filtering in the cavity to compensate for the modal dispersion, similar to the concept of compensating large cavity dispersion by spectral filtering [19]. Figure 2(a) shows a typical waveform of the generated QS pulses with a pump power of 6.7 W in our experiment. The repetition rate of the QS pulses is 70.14 kHz and the pulse width is 1.88 μs with 215.8 mW output power, corresponding to a single pulse energy of 3.08 μJ. The measured RF signal and the beam profile are shown in Fig. 2(b), the right inset of which is the radio frequency spanning from 50 to 500 kHz. The beam pattern indicates the multimode property of the QS state.

To verify the features of the multimode QS, the pump power is decreased to 6.0 W (the threshold power for the QS regime corresponding to a certain NPR state and spatial filtering) and then raised to 8.0 W with a step of 0.1 W. The output power and corresponding repetition rate are, respectively, displayed in Figs. 2(c) and 2(d). It is clear that both

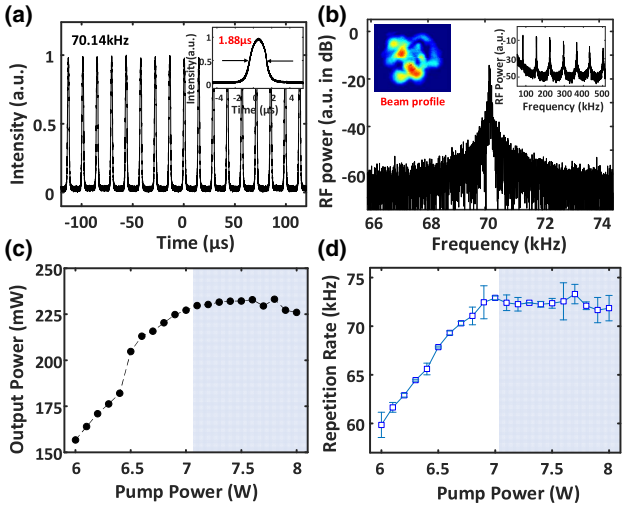

Fig. 2. (a), (b) Typical steady multimode QS pulse train generated in the MMF cavity. (a) QS pulse train with a repetition of 70.14 kHz. The inset shows the corresponding pulse width of 1.88 μs. (b) Corresponding RF spectrum of the QS state (resolution bandwidth: 10 Hz). Left inset: beam profile; right inset: RF spectrum from 0 to 500 kHz. (c) QS output power and (d) repetition rate versus pump power ranging from 6.0 W to 8.0 W. Error bars in (d) shows the repetition rate variation range of the QS pulses.

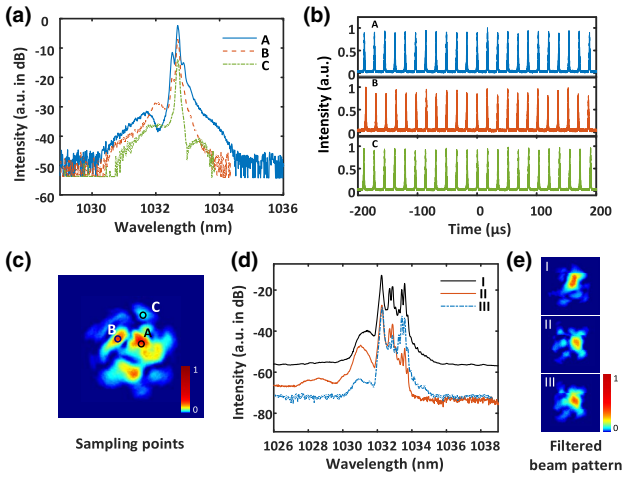

Fig. 3. Characterization of the multimode QS state using (a)–(c) spatial sampling and (d), (e) spectral filtering. (a) Spectra measured at three different points of the output beam by spatial sampling, which are visualized and marked in (c). (b) Corresponding temporal signals (from top to bottom are pulse trains detected at points A, B, and C, respectively, as indicated by their colors). (d) Spectra of the filtered output beam, showing different spectral components. (e) Corresponding beam profiles of the spectral filtered output light.

the output power and the repetition rate rise when the pump power is increased from 6.0 W to 7.0 W. Correspondingly, the pulse width slightly declines from 1.92 μs to 1.81 μs. These results conform to the typical laws of QS regimes. Nevertheless, the repetition rate along with the output power appears to have reached the upper limit with an even higher pump power level [see the blue area in Figs. 2(c) and 2(d)], which is probably a consequence of the saturation of gain fiber. In addition, the QS state in the multimode fiber cavity tends to be unstable (a variation of the repetition rates) at some pump power levels, especially in the range above 7.0 W [See the repetition rate error bars in Fig. 2(d)].

To further verify the multimode properties of the QS states, we measure the output with spatial sampling and spectral filtering following the same method proposed in the literature [19,22,27]. Specifically, for the spatial sampling, the characterization of the output beam is conducted here by using a spatial sampler (e.g., a segment of fiber with a large numerical aperture) fixed on a three-axis stage to collect a small portion of the output light; for the spectral filtering, a set of bandpass filters with different pass bands are used to diminish certain modes with specific spectral components. In multimode fiber lasers, different spatial parts of the beam consist of different superposition of the transverse modes. On the other hand, different transverse modes generally have diverse spectra.

Figures 3(a) and 3(b) display the spectra and the corresponding pulse trains of spatial sampling of the QS laser beam at three different positions. Figure 3(c) visually shows in detail where the light is collected, marked by black dots. It is obvious that the spectra of light collected from points A, B, and C differ from each other. Inferring from Fig. 3(b), the temporal waveform of the QS regime belonging to different transverse modes (or modes combination) is synchronized, which is similar to that in an STML regime [19,22]. The measured spectra and beam profiles after spectral filtering are displayed in Figs. 3(d) and 3(e), respectively. Among the three curves, curve I represents the original spectrum of the output, while curves II and III are the filtered spectra using two bandpass filters working at different wavelengths. Also, the beam pattern varies in different spectral filtering circumstances, which indicates that the output beam is multimode. Note that the two methods for multimode property verification—namely, spatial sampling and spectral filtering—were used in two different QS pulsing regimes. Therefore, the spectra and beam profiles are distinct, which still supports the confirmation of multimode QS states.

B. Transition between Multimode QS and STML

As mentioned above, to maintain stable QS states, it is necessary to obtain a high enough output power (or intracavity power) by optimizing the coupling between the light path in the multimode fibers and the free space, where weak spatial filtering confinement probably facilitates multimode QS generation. On the other hand, according to our experiment, if the light coupling is not as ideal as that of the previous setting already demonstrated to achieve QS (equivalent to a middle-size spatial filter), both STML and multimode QS can be achieved in the same cavity by adjusting the rotation angles of the waveplates. In other words, the STML and QS are supported simultaneously in the fiber laser cavity with a fixed pump power. Moreover, in certain cases, the transition between QS and STML can be achieved by merely altering the pump power. We note this kind of transition via pump power tuning is only supported with a specific cavity setup (i.e., SA, spatial filtering and light coupling), which possibly relies on the multimode gain response as well as the NPR-based SA effect.

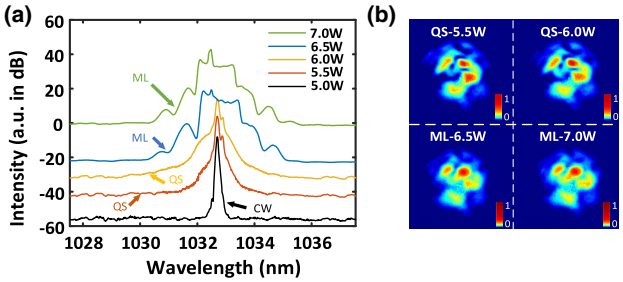

Fig. 4. Transition between QS and STML versus pump power changes. (a) Spectra of the laser output with increasing pump power, covering the CW, QS, and ML operating regimes. (b) Corresponding beam pattern with respect to four different pump power levels, as shown in Visualization 1. The operating regimes and the corresponding pump power are notated in the figures.

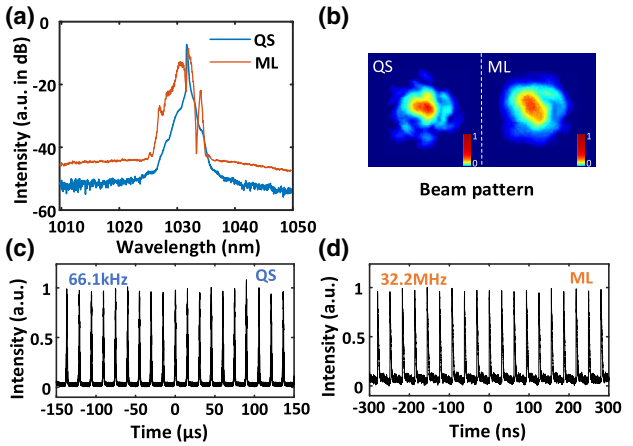

Fig. 5. Typical multimode QS–ML bistable state, shown in Visualization 2. (a) Spectra of QS and ML states and the corresponding (b) beam profiles and (c), (d) pulse trains, with repetition rates of 66.1 kHz and 32.2 MHz, respectively.

Figure 4(a) shows the recorded spectra versus raising the pump power levels from 5 to 7 W with a 0.5 W step, illustrating the transition. To avoid overlap, the acquired spectral data are separated by a 10 dB space. As delineated in Fig. 4, the laser is initially in a CW operating regime while it evolves to a QS state (confirmed by the pulse train measurement) with the increasing pump power. The beam profile does not vary much when the laser transforms from CW to QS, except for minor intensity changes. With the power continuing to ascend, the laser transforms from a QS to an ML state at 6.5 W and keeps ML with increasing power to 7.0 W. We further investigate the achieved ML state with spatial sampling and spectral filtering methods previously mentioned, having confirmed it as an STML state. The corresponding beam profiles of QS and ML states are displayed in Fig. 4(b). As a matter of fact, mode profiles do not differ a lot with different pump powers as long as the laser's operating regime (QS or ML) does not change. Therefore, the beam profiles of QS at a pump power of 5.5 W and 6.0 W as well as those of ML at 6.5 W and 7.0 W are almost identical except for minor differences regarding mode power variation. However, the distinction of the mode profiles between QS and ML regimes is prominent. (See the contrastive beam profiles in Visualization 1.) Note that the measurements are carried out in the case where the NPR state (the rotation angles of three waveplates) stays unchanged. Otherwise, the mode pattern will definitely change a lot, which is not the same operating status within the QS or ML regime. Moreover, the ML state will transform back to QS if the pump power decreases, enabling a reversible transition between the two regimes. Hysteresis of the transition also is observed in our experiment. For the same state shown in Fig. 4, for example, the threshold for QS to ML is around 6.5 W, while the threshold for ML to QS is around 6.1 W. In addition, if the pump power continues to increase above 7 W, the operating regime of the multimode fiber laser tends to be stochastic and even the generated pulses become unstable.

C. Bistability between Multimode QS and STML

It is noteworthy that the laser operating regime can spontaneously switch between multimode QS and STML without any tuning of the cavity with a certain cavity setup (appropriate spatial coupling state, waveplate sets, and pump power). Specifically speaking, the multimode cavity exactly supports a bistable state between multimode QS and ML at a critical pump power level, as shown in Visualization 2. In the experiment in which the bistability occurs, the pump power is first tuned to 5.5 W, a relatively low level where stable QS exists. Only by slightly raising the pump power to 6.5 W, a multimode QS–ML bistable state suddenly appears, as shown in Fig. 5. It is evident that both the spectrum and the beam profile (representing the mode components) change significantly, which are displayed in Figs. 5(a) and 5(b), respectively. The corresponding pulse trains of QS and ML are displayed in Figs. 5(c) and 5(d), with distinct repetition rates of 66.1 kHz and 32.2 MHz. The latter value agrees with the cavity fundamental repetition rate. The bistability is relatively robust and can last for several minutes without any manual control or feedback in our experiment. However, ambient perturbation such as a temperature and pump power fluctuation as well as mechanical vibration noises caused by working devices will pose a potential threat to the existence of the bistable state. Interestingly, hysteresis is not obvious in this case. This bistable state can degenerate into stable ML or QS, for example, by changing the pump power, but will recover if the pump power returns to the original power level (6.5 W in our experiment) as long as the environmental conditions and cavity parameters stay unchanged. The beam profiles and the spectra of the QS and ML will recover to what they previously were. This bistable state is closely related to the pump power while strongly relying on appropriate cavity spatial coupling and the NPR states in our experiment. Transverse mode interactions and the relaxation response of the gain medium might play significant roles in the state-switching behavior.

4. DISCUSSION AND CONCLUSION

Note that the underlying mechanisms of the transition as well as the bistability between multimode QS and STML are more involved than those in single transverse-mode lasers [10,11]

since the participation of spatial (transverse) modes pushes the laser into a higher dimensional category [i.e., three-dimensional (3D)] which naturally complicates the transition dynamics. For example, the hysteresis of the QS–ML transition shows prominent distinction compared to that in single-mode platforms. In some cases (e.g., certain NPR states and cavity setup) in our experiment, the hysteresis is obvious. In other circumstances, however, hysteresis can rarely be observed (e.g., the bistable state shown in Fig. 5). Our demonstration of QS, multimode QS–ML transition, and the bistability has enriched the discovery of the curious properties and dynamics of 3D lasers. Spatiotemporal interactions (i.e., competition and compromise) among SA, the spatial filter, and the gain effect play significant roles in determining the operating regimes as well as the state evolution (i.e., transition, instabilities, and bistable states) of the multimode fiber laser. Spatial mode-resolved measurements and a real-time characterization must be carried out to fully understand the links between multimode QS and STML in future works.

In conclusion, we report the observation of multimode QS and STML in a multimode fiber laser. Multimode QS regimes are more likely to be supported with better cavity spatial coupling equivalent to a larger spatial filter size, according to our experiment. In addition, we have achieved a reversible QS–ML transition, which is strongly dependent on the pump power with a fixed cavity configuration. Furthermore, a critical bistability between the multimode QS and STML is realized under appropriate cavity spatial coupling and NPR states. The demonstration of multimode QS pulses generation and STML in multimode fiber cavities not only provides a promising and feasible way toward high-energy pulse engineering in fiber systems, but also sheds some light on the complex dynamics in 3D lasers concerning QS and ML buildup and evolution.

Funding. National Natural Science Foundation of China (51527901, 61975090); National Key Scientific Instrument and Equipment Development Projects of China (2014YQ510403); State Key Laboratory of IPOC (BUPT), China (IPOC2020ZT02).

Disclosures. The authors declare no conflicts of interest.

REFERENCES

1. O. Svelto, *Principles of Lasers* (Plenum, 1998).
2. G. P. Agrawal, *Applications of Nonlinear Fiber Optics* (Academic, 2008).
3. U. Keller, K. J. Weingarten, F. X. Kartner, D. Kopf, B. Braun, I. D. Jung, R. Fluck, C. Honninger, N. Matuschek, and J. A. D. Au, "Semiconductor saturable absorber mirrors (SESAM's) for femtosecond to nanosecond pulse generation in solid-state lasers," IEEE J. Sel. Top. Quantum Electron. **2**, 435–453 (1996).
4. R. Paschotta, R. Haring, E. Gini, H. Melchior, U. Keller, H. L. Offerhaus, and D. J. Richardson, "Passively *Q*-switched 0.1-mJ fiber laser system at 1.53 μm," Opt. Lett. **24**, 388–390 (1999).
5. D. Popa, Z. Sun, T. Hasan, F. Torrisi, F. Wang, and A. C. Ferrari, "Graphene *Q*-switched, tunable fiber laser," Appl. Phys. Lett. **98**, 073106 (2011).
6. B. Fu, P. Wang, Y. Li, M. Condorelli, E. Fazio, J. Sun, L. Xu, V. Scardaci, and G. Compagnini, "Passively *Q*-switched Yb-doped all-fiber laser based on Ag nanoplates as saturable absorber," Nanophotonics **9**, 3873–3880 (2020).
7. I. N. Duling, "All-fiber ring soliton laser mode locked with a nonlinear mirror," Opt. Lett. **16**, 539–541 (1991).
8. F. Wang, A. G. Rozhin, V. Scardaci, Z. Sun, F. Hennrich, I. H. White, W. I. Milne, and A. C. Ferrari, "Wideband-tuneable, nanotube mode-locked, fibre laser," Nat. Nanotechnol. **3**, 738–742 (2008).
9. Z. Sun, T. Hasan, F. Torrisi, D. Popa, G. Privitera, F. Wang, F. Bonaccorso, D. M. Basko, and A. C. Ferrari, "Graphene mode-locked ultrafast laser," ACS Nano **4**, 803–810 (2010).
10. A. Komarov, H. Leblond, and F. Sanchez, "Theoretical analysis of the operating regime of a passively-mode-locked fiber laser through nonlinear polarization rotation," Phys. Rev. A **72**, 063811 (2005).
11. X. Liu, D. Popa, and N. Akhmediev, "Revealing the transition dynamics from *Q* switching to mode locking in a soliton laser," Phys. Rev. Lett. **123**, 093901 (2019).
12. M. Wohlmuth, C. Pflaum, K. Altmann, M. Paster, and C. Hahn, "Dynamic multimode analysis of *Q*-switched solid state laser cavities," Opt. Express **17**, 17303–17316 (2009).
13. F. Feng and C. Pflaum, "Modeling passively *Q*-switched solid state lasers with multimode," Appl. Math. Modell. **38**, 6052–6065 (2014).
14. S. M. Han, K. Yang, Z. H. Wang, Y. G. Liu, and Z. Wang, "Multimode oscillation *Q*-switched erbium-doped fiber laser with a few-mode fiber cavity," Optoelectron. Lett. **14**, 417–420 (2018).
15. S. Fu, Q. Sheng, X. Zhu, W. Shi, J. Yao, G. Shi, R. A. Norwood, and N. Peyghambarian, "Passive *Q*-switching of an all-fiber laser induced by the Kerr effect of multimode interference," Opt. Express **23**, 17255–17262 (2015).
16. E. Nazemosadat and A. Mafi, "Nonlinear multimodal interference and saturable absorption using a short graded-index multimode optical fiber," J. Opt. Soc. Am. B **30**, 1357–1367 (2013).
17. Z. Wang, D. N. Wang, F. Yang, L. Li, C. Zhao, B. Xu, S. Jin, S. Cao, and Z. Fang, "Er-doped mode-locked fiber laser with a hybrid structure of a step-index–graded-index multimode fiber as the saturable absorber," J. Lightwave Technol. **35**, 5280–5285 (2017).
18. K. Zhao, H. Jia, P. Wang, J. Guo, X. Xiao, and C. Yang, "Free-running dual-comb fiber laser mode-locked by nonlinear multimode interference," Opt. Lett. **44**, 4323–4326 (2019).
19. L. G. Wright, D. N. Christodoulides, and F. W. Wise, "Spatiotemporal mode-locking in multimode fiber lasers," Science **358**, 94–97 (2017).
20. H. Qin, X. Xiao, P. Wang, and C. Yang, "Observation of soliton molecules in a spatiotemporal mode-locked multimode fiber laser," Opt. Lett. **43**, 1982–1985 (2018).
21. U. Teğin, E. Kakkava, B. Rahmani, D. Psaltis, and C. Moser, "Spatiotemporal self-similar fiber laser," Optica **6**, 1412–1415 (2019).
22. Y. Ding, X. Xiao, P. Wang, and C. Yang, "Multiple-soliton in spatiotemporal mode-locked multimode fiber lasers," Opt. Express **27**, 11435–11446 (2019).
23. H. Wu, W. Lin, Y. J. Tan, H. Cui, Z. C. Luo, W. C. Xu, and A. P. Luo, "Pulses with switchable wavelengths and hysteresis in an all-fiber spatio-temporal mode-locked laser," Appl. Phys. Express **13**, 022008 (2020).
24. U. Teğin, E. Kakkava, B. Rahmani, D. Psaltis, and C. Moser, "Dispersion-managed soliton multimode fiber laser," in Conference on Lasers and Electro-Optics (2020), paper SM4P.1.
25. T. Mayteevarunyoo, B. A. Malomed, and D. V. Skryabin, "Spatiotemporal dissipative solitons and vortices in a multi-transverse-mode fiber laser," Opt. Express **27**, 37364–37373 (2019).
26. U. Teğin, B. Rahmani, E. Kakkava, D. Psaltis, and C. Moser, "All-fiber spatiotemporally mode-locked laser with multimode fiber-based filtering," Opt. Express **28**, 23433–23438 (2020).
27. Y. Ding, X. Xiao, K. Liu, S. Fan, X. Zhang, and C. Yang, "Spatiotemporal dynamics of mode locking in multimode lasers with large modal dispersion," arXiv:1912.00161 (2019).
28. U. Teğin, B. Rahmani, E. Kakkava, D. Psaltis, and C. Moser, "Single mode output by controlling the spatiotemporal nonlinearities in mode-locked femtosecond multimode fiber lasers," Adv. Photon. **2**, 056005 (2020).
29. L. G. Wright, P. Sidorenko, H. Pourbeyram, Z. M. Ziegler, A. Isichenko, B. A. Malomed, C. R. Menyuk, D. N. Christodoulides, and F. W. Wise, "Mechanisms of spatiotemporal mode-locking," Nat. Phys. **16**, 565–570 (2020).